Localization of singularities in inviscid limit — numerical examples

Hisashi Okamoto

1 Introduction

We consider a family of stationary Navier-Stokes flows parameterized by the Reynolds number. When the Reynolds number tends to infinity, what asymptotic behaviors are observed? This is the problem which we would like to address in the present paper.

The most renowned phenomenon is the appearance of the boundary layer. This is well-known. However, what happens in the flow region away from the boundary is much less understood. DiPerna-Majda's concentration ([2]) is one example of singular behavior. Another example, which is less singular than concentration, is found in Kolmogorov flows, see [7]. In the present paper we add two examples whose singularities are less singular than concentration but more singular than the internal layer ([7]) in Kolmogorov flows. The singularity means those which appear as asymptotic behaviors in the limit of $R \to +\infty$ (or $\nu \to 0$).

Our examples are Jeffery-Hamel flows([9]) and Oseen's flows ([8]). One of the features of these examples is that the family of steady-states has a definite limit as $R \to \infty$ but the limit functions have discontinuities although all the given data are C^∞ smooth. The degree of discontinuities and localization of singularities depend on individual problems, showing variety of interpretations. We hope such interpretations are helpful in understanding the increase of complexity of fluid flows for large Reynolds numbers.

2 Jeffery-Hamel flow

The Jeffery-Hamel flows are the exact solutions of the Navier-Stokes equations in the two dimensional domain bounded by two semi-infinite lines joining at a point. We study the solutions from the viewpoint of the bifurcation theory.

Let Ω_α denote the following domain:

$$\Omega_\alpha = \{(r, \theta)\ ;\ 0 < r < \infty,\ -\alpha < \theta < \alpha\ \},$$

where (r, θ) is the plane polar coordinates and α is a constant between 0 and π. In this

domain, we consider the stationary Navier-Stokes equations:

$$\begin{aligned} u_r\frac{\partial u_r}{\partial r}+\frac{u_\theta}{r}\frac{\partial u_r}{\partial \theta}-\frac{u_\theta^2}{r} &= \nu\left(\triangle u_r-\frac{u_r}{r^2}-\frac{2}{r^2}\frac{\partial u_\theta}{\partial\theta}\right)-\frac{1}{\rho}\frac{\partial p}{\partial r} \\ u_r\frac{\partial u_\theta}{\partial r}+\frac{u_\theta}{r}\frac{\partial u_\theta}{\partial \theta}+\frac{u_r u_\theta}{r} &= \nu\left(\triangle u_\theta-\frac{u_\theta}{r^2}+\frac{2}{r^2}\frac{\partial u_r}{\partial\theta}\right)-\frac{1}{\rho r}\frac{\partial p}{\partial \theta} \\ \frac{\partial (ru_r)}{\partial r}+\frac{\partial (ru_\theta)}{\partial\theta} &= 0 \end{aligned}$$

with the boundary condition $(u_r, u_\theta)|_{\theta=\pm\alpha} = (0,0)$. Here ν is the kinematic viscosity and ρ is the constant mass density. Jeffery and Hamel showed that all the requirements are satisfied if we put

$$u_r = \frac{\nu g(\theta)}{r}, \qquad u_\theta \equiv 0, \qquad p = \frac{4\rho\nu^2(g(\theta)-b_0)}{2r^2},$$

where g is a function of θ only and b_0 is a constant, and if the function $g = g(\theta)$ satisfies

$$g''+4g+g^2 = b_0 \qquad\qquad (-\alpha<\theta<\alpha) \tag{1}$$

and

$$g(\pm\alpha) = 0. \tag{2}$$

Thus, the set of nonlinear equations are reduced to a two-point boundary value problem of an ordinary differential equation of second order. The unknown constant b_0 is determined by specifying the flux

$$Q = \int_{-\alpha}^{\alpha} u_r(r,\theta) r d\theta = \nu\int_{-\alpha}^{\alpha} g(\theta)d\theta. \tag{3}$$

For given α and Q/ν, any solution of (1), (2) and (3) is called the Jeffery-Hamel flow. In what follows, we call Q/ν the Reynolds number and it is denoted by R.

Let us briefly describe the history of the problem. The discovery of those solutions are credited to [5] and [4]. However, von Kármán [12] claims that he discovered those a year before [4]. Although Jeffery and Hamel independently found some solutions, the whole picture of the solutions were understood only after Rosenhead [9] showed multiple existence of the solutions. Since then, the theory of Jeffery-Hamel flows seems to have been considered to be complete until Sobey and Drazin [11] computed some bifurcation diagrams of the solutions. The study was followed by [1] and bifurcation pictures were shown by numerical computations. As is easily seen, any solution of the equation (1) can be represented in terms of elliptic functions. It is rather surprising that for any given $\alpha \in (0,\pi)$ and $Q/\nu \in \mathbf{R}$, there exists infinite number of solutions satisfying (1,2,3). This unexpected fact was proved by Rosenhead [9]. See Berker [13] for more details. However, classical papers on Jeffery-Hamel flows lacked the viewpoint of bifurcation equations, with which [11] and [1] computed the solutions and found some bifurcation points including, pitchfork, turning points, and cusps. This is an interesting discovery but the main concern of those papers seems to be more in the applications of the Jeffery-Hamel flows to diverging channel flows rather than the complete classification of the Jeffery-Hamel flows. Other interesting features of the Jeffery-Hamel flows are also discussed in [3]. We wish to supply the data which were not presented in these papers. Specifically, we pay attention to the solutions of large Reynolds numbers.

As is noted above, all the solutions can be represented by the elliptic functions. However, it does not immediately tell the qualitative properties of the solutions. Consequently we forget about elliptic functions and we deal with the problem by a purely numerical computation. Since the problem can be viewed as a bifurcation problem, we computed solutions by H.B. Keller's method [6]. The numerical schemes are described in section 4.

3 Properties of the flows

This section presents the numerical results. We study how the solutions bifurcate when the Reynolds number $R = Q/\nu$ changes. Note that R can be both positive and negative.

Figure 1 is the bifurcation diagram we obtained numerically. It consists of two branches. One branch passes through the origin, which we call the main branch, and the other is a secondary branch which bifurcates from the main branch through a pitchfork. The origin represents the trivial solution $R = 0, g \equiv 0$. Starting from this trivial solution, we traced the branch numerically. The main branch has a turning point approximately at $R \approx 11.758$. The secondary branch bifurcates at $R = 9.112\cdots$. The bifurcation is a subcritical pitchfork. Both branches extend to $R \to -\infty$.

The flow patterns change in a very interesting manner. This is known in [9]. But we explain the pattern change for convenience of the reader. Along the main branch AO, the flows are pure inflows, which mean that $g(\theta) < 0$ for all $\theta \in (-\alpha, \alpha)$. A typical pattern is given in Figure 2 (left). Along OB, the flows are pure outflow, i.e., $g(\theta) > 0$ for all $\theta \in (-\alpha, \alpha)$. A velocity pattern is shown in Figure 2 (middle). At the bifurcation point B, it holds that $g'(\pm\alpha) = 0$ (Figure 2 (right)). Along BCD, the flow consists of two inflows and an outflow (Figure 3). All the solutions of the main branch is symmetric about the axis $\theta = 0$. The flows on the secondary branch, however, are asymmetric as is seen from Figure 3(right). The flows on the opposite side of the secondary branch are obtained by reflecting the solutions with respect to the axis $\theta = 0$.

We now consider an interesting question: what asymptotic properties can be seen on the flow patterns if $R \to -\infty$? Note that there are four different curves extending to $-\infty$; the upper and the lower curves of the main branch and two curves on the secondary branch. So, we consider the problem for individual curves. The two curves of the secondary branch are the same in the sense that they are mapped to each other by the reflection about $\theta = 0$. So, we have to consider three cases. Among these, the case of the lower main branch is well known and mathematically rigorous proof of a certain asymptotic behavior is available ([10]). However, it seems to the author that the two other cases have escaped from the detailed analysis.

Let us begin with the well known case of the lower main branch, the branch containing OA. All the solutions on the lower branch with $R < 0$ are pure inflows. They all share the following properties: (1) g is decreasing in $-\alpha < \theta < 0$, (2) g is increasing in $0 < \theta < \alpha$, (3) g takes its unique minimum at $\theta = 0$, (4) g is convex in $-\alpha < \theta < \alpha$. For the proof, see [10]. The asymptotic property of the solution is known ([10]): (1) $\frac{1}{R}g$ converges to a constant $1/(2\alpha)$, in $-\alpha < \theta < \alpha$, (2) the convergence is uniform in every compact set of $(-\alpha, \alpha)$ but not uniform in $[-\alpha, \alpha]$, What is more interesting is the boundary layer exhibited

by the solutions. If we re-scale g as

$$h(x) = \frac{1}{R} g\left(\frac{x}{\sqrt{R}} + \alpha\right), \qquad x \in [0, x_0]$$

then h converges to $b\tanh(ax)$ with a suitable constant, $x_0 > 0$, a, and b, as $R \to -\infty$. For the proof, see [10]. Figure 4 (left) is the flow patterns when $R = -200$, which clearly shows the sharp transition from a nonzero velocity in $|\theta| < \alpha$ to zero at $\theta = \pm\alpha$.

We now turn to the upper main branch, where the flow patterns consists of two inflows near the boundaries and an outflow near the axis $\theta = 0$. Our computation shows the following:

- as R decreases, two inflows widens and the outflow near the center becomes thinner,
- the maximum absolute velocity takes at $\theta = 0$, i.e., in the outflow,
- the outflow looks like a thin jet but the inflows looks like the pure inflows discussed above (Figure 4(middle)).

We next consider the asymmetric solutions on the secondary branch. the flows consist of an inflow and an outflow. As R decreases, the inflow widens and the outflow becomes narrower. As $R \to -\infty$, the inflow behaves asymptotically as the pure inflows discussed above. However, the asymptotic behavior of the outflow part is different. It seems that the width of the outflow becomes smaller and tends to zero as $R \to -\infty$. However, this does not imply the disappearance of the outflow, since the maximum absolute velocity is taken at the outflow part (see Figure 4(right)). So we may conclude that the flow have two different boundary layers the one is the same as that of the well-known pure inflows. The other layer has an inflection point inside the boundary layer. Or we may say that the boundary layer has a reversed jet. Although the boundary jet is the same as the center jet of the upper main branch, its appearance in the boundary layer seems to be interesting.

Finally we remark again that there are an infinite number of solutions for a fixed R. Those solutions constitute curves having turning points. Those branches are disconnected from the branch in Figure 1 and are not drawn there. The solutions in such a branch have more than one inflow and outflow. See Berker [13] or Rosenhead [9] for details.

4 Numerical scheme

We briefly outline our numerical scheme for (1)–(3). We discretize (1) by the Chebyshev-collocation method as follows: Choose a positive integer N and set

$$g_N(\theta) = \sum_{n=1}^{N+1} a(n) T_{n-1}(\theta/\alpha),$$

where $a(n)$ are real coefficients to be determined, and T_{n-1} is the Chebyshev polynomial of order $n-1$. Putting $m = N+2$, we define $F = (F_1, \cdots, F_m)$ as follows:

$$F_1 = g(\alpha) = \sum_{n=1}^{N+1} a(n), \qquad F_2 = g(-\alpha) = \sum_{n=1}^{N+1} (-1)^{n-1} a(n)$$

$$F_3 = \sum_{n=1}^{N+1} a(n) \int_{-\alpha}^{\alpha} T_{n-1}(\theta/\alpha) d\theta - R = \sum_{n=1}^{N+1} \frac{-2\alpha a(n)}{n(n-2)} - R$$

and

$$F_k = g''(\theta_{k-3}) + 4g(\theta_{k-3}) + g(\theta_{k-3})^2 - a_m$$

for $4 \le k \le m$, where θ_{k-3} is defined as $\theta_j = \alpha \cos(\pi j/N)$ and a_m stands for the constant b_0 in (1). Note that F_1 and F_2 come from (2); F_3 comes from (3). We then have a mapping $F = F(R; a_1, a_2, \cdots, a_m)$ from $\mathbf{R}^{m+1}$ to $\mathbf{R}^m$. The two point boundary value problem is now approximated by the problem to find zeros of F.

Since $F(0; 0, \cdots, 0) = (0, \cdots, 0)$, we can trace the solutions by H.B. Keller's method (see [6]). For computations with $|R| < 100.0$, we chose $N = 128$. For a larger $|R|$, we increased N.

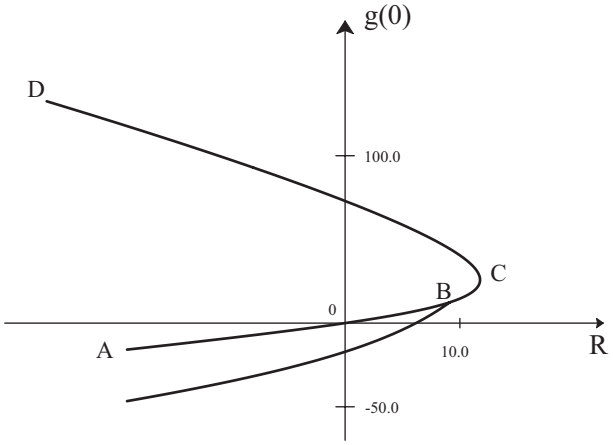

Figure 1: Bifurcation diagram of Jeffery-Hamel flows: $\alpha = \pi/4$.

As we have shown, some solutions have a sharp internal layer. The numerical scheme above is no longer effective for such solutions with internal layers. For a symmetric solutions, only the knowledge of those part where $0 < \theta < \alpha$ is sufficient. In this case we computes g satisfying

$$g'' + 4g + g^2 = b_0 \qquad (0 < \theta < \alpha) \tag{4}$$

and $g'(0) = 0$, $g(\alpha) = 0$. Expanding g by a Chebyshev series in $[0, \alpha]$, we obtain a similar scheme. Only in this way we can compute solutions having a internal jet with $R < -200$.

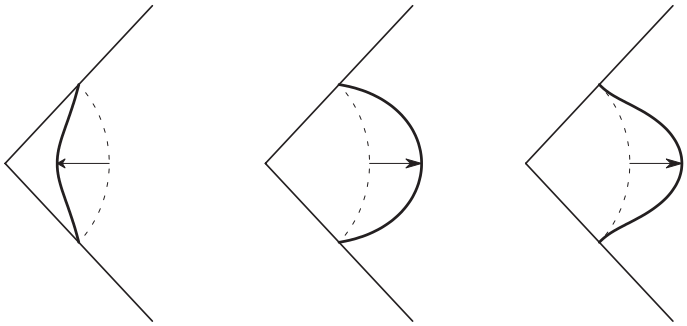

Figure 2: Velocity profile: $\alpha = \pi/4$. $R = -10.0$ (left), $R = 3.0$(middle), and $R = 9.112$(right).

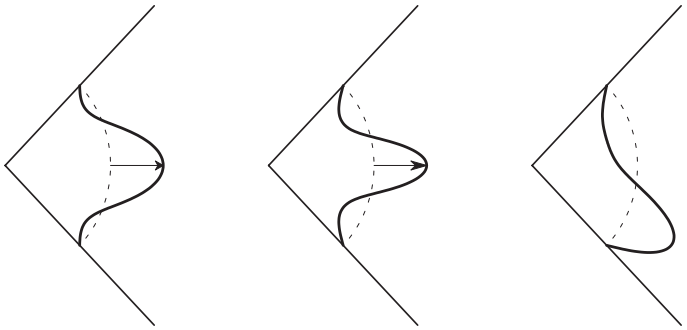

Figure 3: Velocity profile: $\alpha = \pi/4$. $R = 11.5$ (left) and $R = 0$ (middle and right).

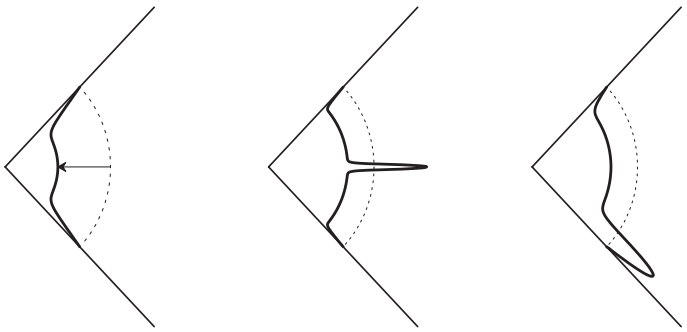

Figure 4: Velocity profiles. $R = -200$ (left), $R = -10000.0$ (middle), $R = -400.0$ (right).

5 Oseen's flow

Oseen discovered in his paper [8] a family of stationary solutions of the Navier-Stokes equations. His solutions are re-examined here as a bifurcation problem and flow patterns are computed for large Reynolds numbers.

The stationary solutions of the Navier-Stokes equations in the plane are considered:

$$(\mathbf{u}\cdot\nabla)\mathbf{u} = \nu\triangle\mathbf{u} - \frac{1}{\rho}\nabla p, \qquad \operatorname{div}\mathbf{u} = 0,$$

where $\mathbf{u}$ is the velocity vector, p is the pressure. We consider steady states which is given by a stream function ψ. Namely $\mathbf{u} = (\psi_y, -\psi_x)$. Our standing assumption, which is the same as those assumed by Oseen [8], is that the stream function ψ is of the following form: $\psi = f(\phi) + C\chi$, where C is a constant, f is a function of one variable, and we define ϕ and χ by

$$\phi = B\log r + \theta, \qquad \chi = \log r - B\theta.$$

Here, B is another constant: r and θ are polar coordinates. We require that ψ is smooth except at the origin, that the gradient of ψ is a single-valued function of θ, and that the Navier-Stokes equations are satisfied in $\mathbf{R}^2 \setminus \{0\}$.

We assume the following form of f:

$$f(\phi) = \alpha_0\phi + \sum_{n=1}^{\infty}\alpha_n \sin n\phi \equiv \alpha_0\phi + g(\phi),$$

where α_n $(n = 1, 2, \cdots)$ are constants. Accordingly we have

$$\psi = (\alpha_0 B + C)\log r + (\alpha_0 - CB)\theta + g(\phi). \tag{5}$$

The Navier-Stokes equations written in ψ is:

$$\nu\triangle^2\psi = r^{-1}\left[\psi_\theta(\triangle\psi)_r - \psi_r(\triangle\psi)_\theta\right]. \tag{6}$$

Substituting (5) into (6), we obtain

$$\begin{aligned}\nu\left\{4(1+B^2)g'' - 4B(1+B^2)g''' + (1+B^2)^2 g^{(IV)}\right\}\\ = -2(\alpha_0 - CB)(1+B^2)g'' - C(1+B^2)^2 g''' - 2(1+B^2)g'g''.\end{aligned}$$

We now define U by $g' = -\nu(1+B^2)U$. Then the equation above becomes

$$\frac{4}{1+B^2}U' - \frac{4B}{1+B^2}U'' + U''' = -\frac{2(\alpha_0 - CB)}{1+B^2}U' - \frac{C}{\nu}U'' + 2UU'.$$

This equation can be integrated once and we obtain

$$\frac{4}{1+B^2}U - \frac{4B}{1+B^2}U' + U'' = -\frac{2(\alpha_0 - CB)}{1+B^2}U - \frac{C}{\nu}U' + U^2 + d_0$$

with some constant d_0. In order that this equation possess a solution U which is 2π-periodic, it is necessary to have $C/\nu = 4B/(1+B^2)$, which we will assume henceforth. Thus we finally get to

$$U'' + \left(\frac{4}{1+B^2} + \frac{2(\alpha_0 - CB)}{\nu(1+B^2)} \right) U = U^2 + d_0.$$

The flux along the circle $r = 1$ is

$$\int_0^{2\pi} u_r r d\theta = \int_0^{2\pi} \frac{\partial \psi}{\partial \theta} d\theta = 2\pi(\alpha_0 - CB). \tag{7}$$

Accordingly we define the Reynolds number R by $R = 2\pi\nu^{-1}(\alpha_0 - CB)$. Now the problem is to find a 2π periodic U such that

$$\int_0^{2\pi} U(\phi) d\phi = 0 \tag{8}$$

and

$$U'' + AU = U^2 - \frac{1}{2\pi} \int_0^{2\pi} U(\phi)^2 d\phi. \tag{9}$$

where $A = (4 + R/\pi)/(1 + B^2)$. Once the solution U is obtained, the stream function is given by

$$\frac{\psi}{\nu(1+B^2)} = \frac{R\phi}{2\pi(1+B^2)} + \frac{4B \log r}{1+B^2} - \int_0^{\phi} U. \tag{10}$$

The streamlines $(r(s), \theta(s))$ are the solutions of the following ordinary differential equations:

$$r\dot{r} = \frac{R}{2\pi(1+B^2)} - U(B \log r + \theta), \quad r^2\dot{\theta} = -\frac{B(R+8\pi)}{2\pi(1+B^2)} + BU(B \log r + \theta).$$

6 Solutions of the boundary value problem

The problem of finding solutions to (8) and (9) are considered in this section. Obviously, $U \equiv 0$ is a solution. We consider solutions which bifurcates from this trivial solution. In doing so, A is regarded as a bifurcation parameter and we look for solutions which are even functions of ϕ. By linearizing the equation, we have

$$\int_0^{2\pi} U(\phi) d\phi = 0, \qquad U'' + AU = 0.$$

Thus the bifurcation points are given by $A = n^2$, where n is a positive integers. The eigenfunction corresponding to this is $U = \cos n\phi$.

Note that if $(A, U(\phi))$ is a solution to (8) and (9), then $(n^2 A, n^2 U(n\phi))$ is a solution, too. Thus, we obtain all the bifurcation branches once we get the branch from $(1, 0)$.

Theorem 6.1 *The bifurcation at $(A, U) = (n^2, 0)$ is subcritical.*

Proof: By the remark just before the theorem, we may put $n = 1$. Solutions near $(1, 0)$ are obtained as the following functions parameterized by a small number ϵ:

$$\begin{aligned} A &= 1 + A_1\epsilon + A_2\epsilon^2 + \cdots \\ U &= \epsilon U_1 + \epsilon^2 U_2 + \cdots . \end{aligned}$$

Substituting these equations into (8) and (9), we see that each U_k satisfies $\int_0^{2\pi} U_k(\phi)d\phi = 0$ and that

$$U_1'' + U_1 = 0, \tag{11}$$

$$U_2'' + U_2 + A_1 U_1 = U_1^2 - \int_0^{2\pi} U_1(\phi)^2 d\phi, \tag{12}$$

$$U_3'' + U_3 + A_1 U_2 + A_2 U_1 = 2U_1 U_2 - \int_0^{2\pi} 2U_1(\phi)U_2(\phi)d\phi. \tag{13}$$

The equation (11) gives $U_1 = \cos\phi$. In order that the equation (12) is solvable with respect to U_2, it is necessary and sufficient that the integral on $0 \le \phi < 2\pi$ of the equation multiplied by U_1 vanish. This gives that $A_1 = 0$. The equation (12) and $A_1 = 0$ give us

$$U_2 = -\frac{1}{6}\cos 2\phi.$$

By the solvability of (13) with respect to U_3, we obtain

$$A_2 \int_0^{2\pi} U_1^2 d\phi = 2\int_0^{2\pi} U_1^2 U_2 d\phi,$$

which gives us $A_2 = -1/6$. Accordingly, the bifurcation is subcritical.

□

We computed solutions of (8) and (9) by a spectral method as follows. With a positive integer N, we put

$$U_N = \sum_{k=1}^{N} a_k \cos k\phi.$$

The unknowns $\{a_k\}_{k=1}^N$ are determined as the zeros of $F = (F_1, F_2, \cdots, F_N)$, where

$$F_k(A; a_1, a_2, \cdots, a_N) = (U_N'' + AU_N, \cos k\phi) - \left(U_N^2, \cos k\phi\right) \qquad (1 \le k \le N),$$

where $(\ ,\ )$ denotes the L^2 inner-product. The computed branch of solutions of mode one is depicted in Figure 5.

7 Flows of closed streamlines

We first consider the case where $R = 0$. Note that $R = 0$ is equivalent to the single-valuedness of ψ (see (7)). Since $A = 4/(1 + B^2)$, only those solutions of (8) and (9) satisfying either $n = 1$, $0 < A \leq 1$ or $n \geq 2$, $0 < A \leq 4$ can be used. We first prove that all the streamlines of any solutions are closed if $R = 0$ and $B \neq 0$:

Lemma 7.1 *Suppose that $R = 0$ and $B \neq 0$. Then any streamline of any solution is closed. It encloses the origin inside.*

Proof: By (10), we easily see that $\nabla\psi$ vanishes nowhere in $\mathbf{R}^2 \setminus \{0\}$. On the other hand, $\int_0^\phi U$ is a bounded function. Thus,

$$\psi \sim \frac{4B}{1 + B^2} \log r \qquad \text{as } r \to 0, \infty.$$

The conclusion follows from these observations.

□

Since $\phi = B \log r + \theta$, it holds that

$$\psi(\rho r, \theta - B \log \rho) = \psi(r, \theta) + C(1 + B^2) \log \rho$$

for all $\rho > 0$. Therefore we can draw all the streamlines if any one of them are drawn. Figures 6–8 show some examples.

When $n \geq 3$, $A = 4.0$ and a non-trivial U is possible as a solution with $R = 0$. In this case, B is zero and the stream function depends on θ, only. The streamlines are straight lines emanating from the origin.

8 Solutions of $R \neq 0$

We now consider the general case where $R \neq 0$. Since $A = (4 + R/\pi)/(1 + B^2)$, any solution of (8) and (9) represents a family of solutions in which A is the same but (R, B) is different. So, we fix B and let R vary.

Lemma 8.1 *For $R \neq 0$, none of the streamlines is closed.*

Proof: By (10) the vector field vanishes nowhere. Therefore, any closed streamline, if it exists, must enclose the origin. On the other hand, the stream function is constant along the streamline. This is a contradiction, since the stream function increases by $R\nu$ (see (10)) when we move along the streamline enclosing the origin.

□

We first consider the case where $B = 0$ and $n = 1$. Since $A = 4 + \pi^{-1}R$, only $R \leq -3\pi$ is admissible. The stream function depends only on θ and all the streamlines are semi-infinite straight lines issuing from the origin. Although the topology of the streamlines are simple, there is an interesting feature in this family. That is the location of outflow and inflow. Figure 9 shows velocity distribution along the unit circle. In a large part of the circle, the flow is inward but the flow is outward near the leftmost part of the circle. This outflow part get thinner as the Reynolds number R tends to $-\infty$. See Figure 9.

We finally consider the case where $B \neq 0$. Since the stream function is not single-valued, we plot contours of $|\mathbf{u}|^2$. Figure 10 shows the case where $B = 2.0$. Figure 11 shows the case where $B = 5.0$.

The y-component of the velocity along the x-axis are plotted in Figure 12. This clearly shows a kind of weak concentration. Note that a larger $|R|$ means thinner jet. Also note that, when $|R|$ is large, the flow is almost uniform except in the neighborhood of the jet.

References

[1] W.H.H. Banks, P.G. Drazin, and M.B. Zaturska, On perturbation of Jeffery-Hamel flow, J. Fluid Mech., vol. 186 (1988), pp 559–581.

[2] R.J. DiPerna and A.J. Majda, Concentrations in regularizations for 2-D incompressible flow, Comm. Pure Appl. Math., vol. 40 (1987), 301–345.

[3] K. Fujimura, On the linear stability of Jeffery-Hamel flow in a convergent channel, J. Phys. Soc. Japan, vol. 51 (1982), pp. 2000–2009.

[4] G. Hamel, Spiralförmige Bewegungen zäher Flüssigkeiten, Jahrsbericht der Deutchen Math.- Vereinigung, vol. 25 (1917), pp. 34–60.

[5] G.B. Jeffery, The two dimensional steady motion of a viscous fluid, Phil. Mag. S.6, vol. 29 (1915), pp. 455–465.

[6] H.B. Keller, Lectures on Numerical Methods in Bifurcation Theory (Tata Institute of Fundamental Research No. 79), Springer Verlag, (1987).

[7] H. Okamoto, Nearly singular two-dimensional Kolmogorov flows for large Reynolds number, J. Dynamics and Diff. Eqns., vol. 8 (1996), pp. 203–220.

[8] C. W. Oseen, Exakte Lösungen der hydrodynamischen Differentialgleichungen. I., Arkiv Mat. Astr. Fysik, vol. 20 (1927–1928), No. 14, pp. 1-14: ibid. II., ibid, No. 22, 1–9.

[9] L. Rosenhead, The steady two-dimensional radial flow of viscous fluid between two inclined plane walls, Proc. R. Soc. Lond. A, vol. 175 (1940), pp 436–467.

[10] J. Serrin, On the mathematical basis for Prandtl's boundary layer theory: an example, Arch. Rat. Mech. Anal., vol. 28 (1968), pp. 217–225.

[11] I.J. Sobey and P.G. Drazin, Bifurcation of two dimensional channel flows, J. Fluid Mech., vol. 171 (1986), pp. 263–287.

[12] T. von Kármán, The engineer grapples with nonlinear problems, Bull. Amer. Math. Soc., vol. 46 (1940), pp. 615–683.

[13] R. Berker, Intégration des équations du mouvement d'un fluide visqueux incompressible, Handbuch der Physik, vol. VIII/2 (1963), pp. 1–384.

Research Institute for Mathematical Sciences
Kyoto University, Kyoto, 606-01 Japan
okamoto@kurims.kyoto-u.ac.jp

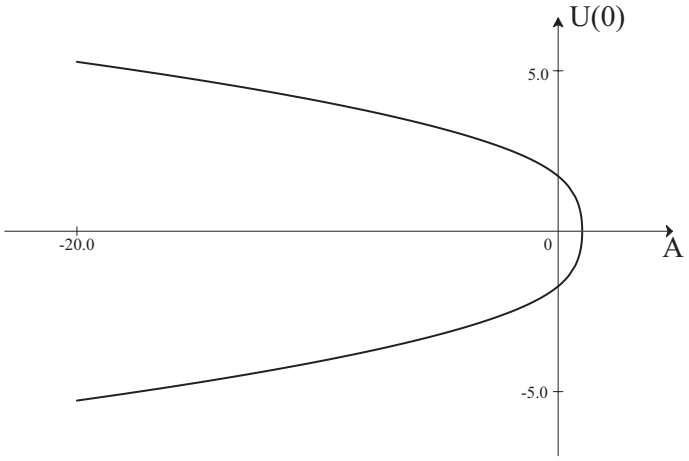

Figure 5: Bifurcation branch of mode 1 ; x-axis represents A and the y-axis does $U(0)$; $N = 100$

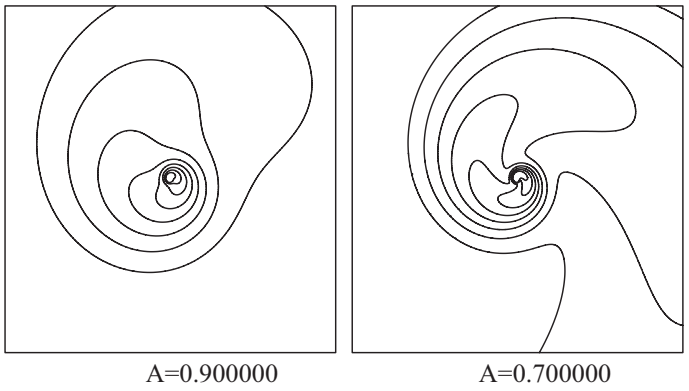

Figure 6: Streamlines: $n = 1, R = 0$; $A = 0.9$ (left) and $A = 0.7$ (right)

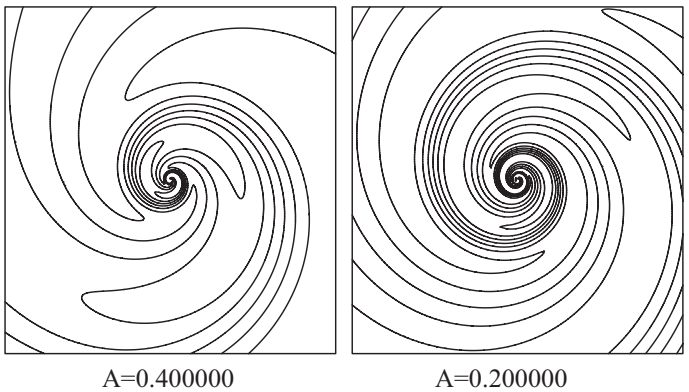

Figure 7: Streamlines: $n = 1, R = 0$; $A = 0.4$ (left) and $A = 0.2$ (right)

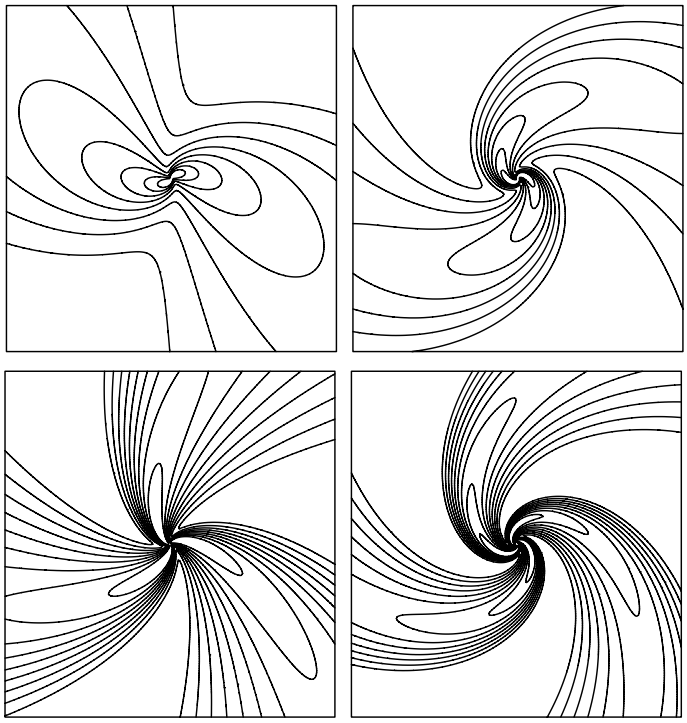

Figure 8: Streamlines: $R = 0$; $n = 2, A = 3.5$ (upper left) ;$n = 2, A = 2.0$ (upper right); $n = 3, A = 3.5$ (lower left), $n = 3, A = 2.0$ (lower right)

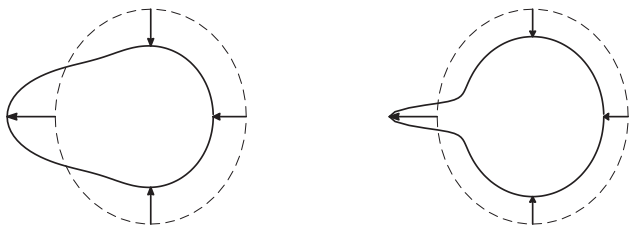

Figure 9: Velocity distribution on circle: $n = 1$; $A = -10.0$ (left) and $A = -300.0$ (right)

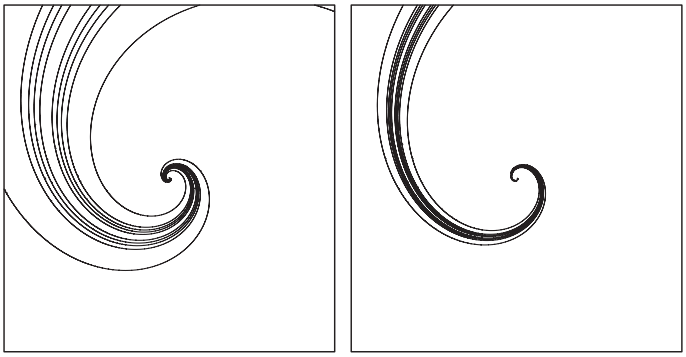

Figure 10: Contours of $|\mathbf{u}|^2$: $n = 1$, $B = 2.0$; $A = -50.0$ (left) and $A = -300.0$ (right)

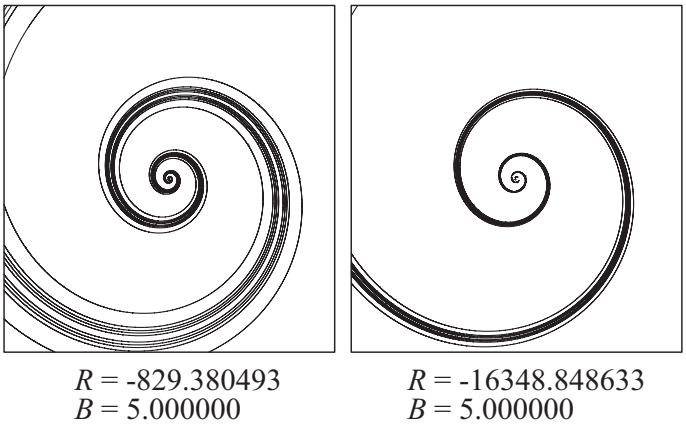

Figure 11: Contours of $|\mathbf{u}|^2$: $n = 1$, $B = 5.0$; $A = -50.0$ (left) and $A = -300.0$ (right)

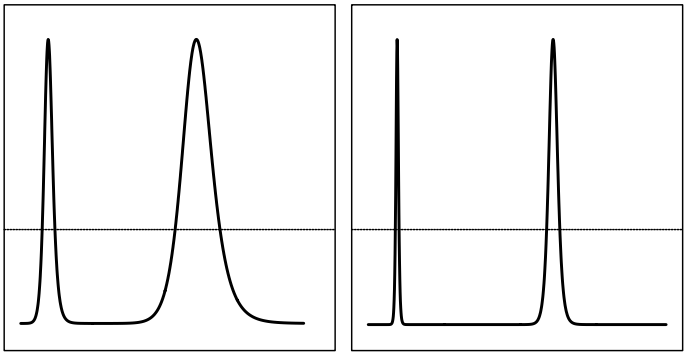

Figure 12: Distribution of the y-component of the velocity on the x-axis: $n = 1, B = 5.0$; $A = -10.0$ and $A = -200.0$. x ranges in $[1, 10]$. The dotted line shows where the y-component is zero.